Sensitivity Study of Fiber Orientation on Stroke Volume in the Human Left Ventricle

Lukas Baron, Thomas Fritz, Gunnar Seemann, Olaf Dössel

Institute of Biomedical Engineering, Karlsruhe Institute of Technology (KIT), Karlsruhe, Germany

Abstract

Orientations of myocytes impact electric excitation propagation and mechanical contraction in the human heart. Measured fiber angles in experiments are obtained from different species (e. g. rat, canine, dog, human heart) and vary by various reasons. It is unclear to what extent non-exact fiber angles impact the quality of computational simulations. In this paper, mechanical simulations with different ventricular angles were performed and compared. The simulations covered the complete heart with both ventricles, both atria and the pericardium and were performed using finite element method. Helix angles were varied between 20° *and* 70° *on endocardium and* -70° *and* -20° *on epicardium. Results showed that fiber orientations had only a minor contribution to the difference between endsystolic and enddiastolic pressure of* $< 8.3\,\%$*. The influence on stroke volume as well as AVPD is significant (changes by* $34\,\%$ *for SV and* $241\,\%$ *for APVD) , but it could not be observed that a higher AVPD yields a higher stroke volume. Concludingly, fiber orientations are important for reliable computational simulations of human hearts and should be incorporated with great care.*

1. Introduction

Evolution has turned blood circulation in the human body into a sophisticated system for supply of cells with oxygen and nutrients. In the middle of the cardiovascular system stands the heart with its pumping function, evoqued by shortening of myocyte fibers.

Fiber orientation angles (FO) measured in experiments rely on various sources like rat, canine, dog and even human hearts. They show a variation not only due to species, but also by individuals and even the methods for computing reference axes differs. Consequently, it is not necessarily possible to derive generically valid angles. According to [1], helix angles, i. e. the angle between the fiber and the long axis of the heart, from -70° on the epicardium to $+50^\circ \ldots + 70^\circ$ on the endocardium depending on the depth within the wall have been observed (see [1], or [2] and references therein).

FO in computational heart models can be integrated mainly using two methods. Inclusion using (a) non-invasive diffusion tensor MRI is preferable, but introduces possibly large inaccuracies by noise. Measuring the diffusion of water molecules in myofibers in the moving heart of alive patients is a possible but challenging and time consuming task [3], [4]. As alternative approach, (b) rule-based methods (RBM) were developed, being able to generate FO just on basis of a few physiological parameters.

Some RBMs are based on assigning regions and parameters by hand, e. g. in the atria [5] and/or use minimum distance functions. [6] and [7] propose algorithms based on solving a Laplace equation to obtain smooth FO. Thereby, [6] is able to generate seamlessly changing FO throughout the whole ventricles, including the septum. The drawback of RBMs is that model-based errors are introduced and a wrong choice of the parameter sets might turn the whole simulations useless. [8] investigated the effect of FO in a rat heart.

In this study, different sets of FO were computed with the algorithm by Bayer et al. [6] and compared using computational simulation of an elastomachanical model of the whole human heart. The influence of different ventricular FO on the pumping function of the heart was determined on the basis of mechanical simulations. The ques-

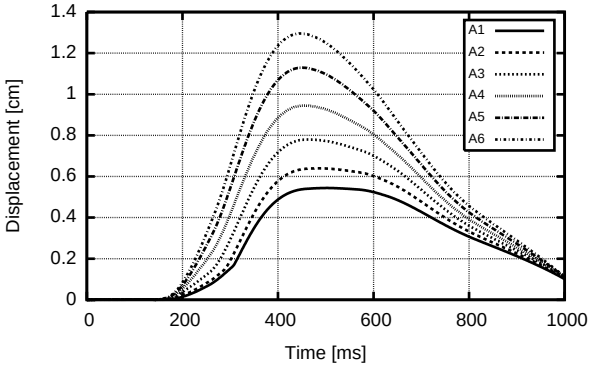

Figure 1. AVPD for the different simulation settings.

tion should be answered, in which way FO impact mechanical behavior of the heart in numerical simulations and up to what degree 'general' fiber angles influence results in a negative way.

2. Methods

2.1. Heart Geometry

The heart geometry was obtained from MRI data of a 32-year-old healthy volunteer at the University Hospital of Heidelberg. It consisted of 11.622 elements with an average element volume of 80 mm^3. It is the same that was used in [9]. FO in the atria were initialized using the semi-automatic method by Krüger et al. [5]. Their algorithm takes 22 seed points as input and constructs a network of auxiliary lines to define FO and cardiac bundles. FO in the ventricles were initialized in all simulations using the algorithm by Bayer et al. [6].

2.2. Elastomechanical Modeling

The elastomechanical simulation framework was presented by Fritz et al. [9]. An electrophysiological model for cellular action potentials by ion channels and concentrations together with a tension development model driven by calcium concentration was used. The excitation propagation was calculated using a monodomain reaction-diffusion model (for details see [9], [10]). The electrophysiology of ventricles was computed only in end-diastolic geometry, without feedback from the deformation. The ventricles were coupled with a three-element Windkessel model to respect blood pressure. Moreover, the method contained a contact handling algorithm to ensure permanent and frictionless contact with the pericardium.

Mechanics and kinematics of the heart were described by the governing equation for balance of linear momentum in its weak total Lagrangian formulation

$$\mathbf{M_{IJ}}\ddot{\mathbf{u}}_\mathbf{J} + \mathbf{f}_\mathbf{I}^{\text{int}} + \mathbf{f}_\mathbf{I}^{\text{cont}} + \mathbf{f}_\mathbf{I}^{\text{circ}} = \mathbf{0} \qquad (1)$$

with mass matrix $\mathbf{M_{IJ}}$, displacement $\mathbf{u_J}$ of node $\mathbf{J}$, internal forces $\mathbf{f}_\mathbf{I}^{\text{int}}$, forces from contact handling algorithm $\mathbf{f}_\mathbf{I}^{\text{cont}}$ and forces from circulatory system $\mathbf{f}_\mathbf{I}^{\text{circ}}$. It was discretized with 10-node tetrahedral elements and endowed with the constitutive material law by Guccione et al. for cardiac tissue [11].

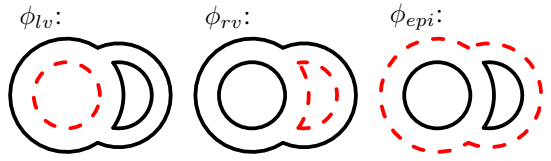

Figure 2. Schematic view from above on the Dirichlet boundary values for the different potentials in the ventricles according to the algorithm by Bayer et al. [6]. Red dashed lines were initialized with a potential of 1, solid black lines with a potential of 0.

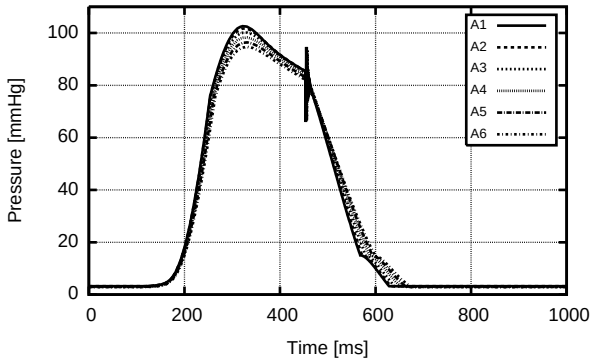

Figure 3. Pressure diagram in the left ventricle for the different simulation settings.

2.3. Fiber Orientations

Fibers in the ventricles were set using the semi-automatic Laplace-Dirichlet rule-based algorithm presented by Bayer et al. [6]. The algorithm takes four angles as input parameters, two describing the helix angle of fibers on the endo- and epicardium and two for the respective sheet angles.

Three different potentials, ϕ_{epi}, ϕ_{lv} and ϕ_{rv}, were computed as solutions of a Laplace equation that differ in the Dirichlet boundary conditions according to Fig. 2. By the choice of boundary values, their absolute values yield transmural depth, depth through the septum and interpolation weights in a natural manner. A forth potential ψ_{ab} for the apicobasal direction got one point on the apex and several points on the base of the heart as Dirichlet boundaries. Their gradients yield local direction vectors that are orthogonalized, rotated according to prescribed angles and subsequently interpolated to obtain one final FO coordinate system. Interpolation of the coordinate systems was done using the 'bislerp' algorithm [6], that is based on spherical linear interpolation (slerp) but respects the special bilinear nature of fiber coordinate systems.

The potentials were computed by solving the Laplace equations

$$\Delta\psi_{ab} = 0, \quad \Delta\phi_{epi} = 0, \quad \Delta\phi_{lv} = 0, \quad \Delta\phi_{rv} = 0$$

using a standard finite element method with tetrahedron elements of first order. That is in contrast to the mechanical simulation, where 10 node tetrahedra were used. The solver used the same mesh, but only 4 corner nodes of each

tetrahedron. Potentials were interpolated from the corner nodes to five Gauss quadrature nodes in the interior for the mechanical simulation. Gradients were computed using the finite element interpolation of the shape function gradients, and thus are constant within each element.

2.4. Simulation Settings

The angles from the paper of [6] served as starting point of the simulations. They optimized the four parameters $(\alpha_{endo}, \alpha_{epi}, \beta_{endo}, \beta_{epi})$ to $(40, -50, -65, 20)$ in order to fit best to data obtained from diffusion MRI. In the simulations performed for this paper, the difference angle between α_{endo} and α_{epi} was kept fixed to $90°$. The endocardial angle was varied in steps of $10°$ in a range of $20°$ to $70°$ and the epicardial angle in the same manner from $-70°$ to $-20°$ as stated in table 1. That is completly within the range of FO measured by Toussaint [4] at a group of 10 healthy volunteers. The parameters β_{endo} and β_{epi} were not used since the simulation did not include a model respecting these values. Electrophysiological excitation propagation was computed only once on a reference set. This was the same electrophysiological configuration as in [9].

2.5. Evaluation Criteria

The results were evaluated by means of two different measures that were also used in [9]: the displacement of the atrioventricular plane (AVPD) and stroke volume in the left ventricle. As additional evaluation, intraventricular pressure difference and pressure volume work per stroke were computed from pV data for the left ventricle and are shown in table 1.

Atrioventricular Plane Displacement (AVPD) was computed using five representative triangles on the left ventricular valve plane. The normal vector was computed in initial state and the displacement measured in that direction for each triangle. AVPD values are the arithmetic mean of single displacements of the five triangles. *Ejection or stroke volume (SV)* of the left ventricle is the difference between enddiastolic (EDV) and endsystolic (ESV) volume. SV was computed in the simulations as the difference between maximal and minimal volumes, according to the formula $SV = EDV - ESV \approx V_{\max} - V_{\min}$. The *pressure difference* was computed in the same manner by $\Delta p = p_{\max} - p_{\min}$. *Pressure volume work (pV work)* is the area included by the pressure volume curve in the pV diagram. It has been computed by integration over time during systole via $W_{pV} = -\int_{V_{\min}}^{V_{\max}} p\, dV$, where $V_{\min}$ and $V_{\max}$ are the endsystolic and enddiastolic volumes, respectively.

Table 1. Fiber angle settings and simulation results.

setting	A1	A2	A3	A4	A5	A6
α_{endo}	20	30	40	50	60	70
α_{epi}	-70	-60	-50	-40	-30	-20
pressure diff [mmHg]	99.4	98.5	97.0	95.2	93.4	91.8
stroke volume [ml]	74.0	73.1	70.1	65.3	60.1	55.2
ejection fraction [%]	53.9	53.3	51.1	47.6	43.8	40.2
pV work in LV [J]	1.51	1.52	1.50	1.47	1.43	1.39
max AVPD [cm]	0.54	0.64	0.78	0.95	1.13	1.30

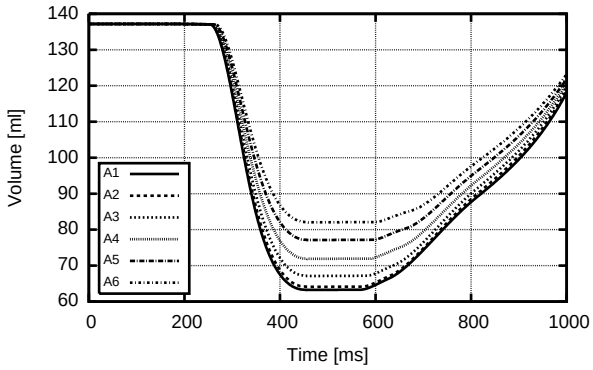

Figure 4. Volume change in the left ventricle for the different simulation settings.

3. Results

From the simulation results, pressure (Fig. 3), volume (Fig. 4) and pV diagrams (Fig. 5) were created for the left ventricle for all FO settings. Moreover, the AVPD is plotted for all performed simulations (Fig. 1). Table 1 shows in the lower part extracted parameters for the simulated settings.

The pressure difference increases constantly with decreasing epicardial angle α_{epi}, that is one with a steeper alignment. The highest value (A1) is $8.3\,\%$ above the lowest (A6). Also stroke volume and ejection fraction constantly increase with decreasing α_{epi}. Here, the highest values (A1) show a $34.0\,\%$ higher output than the lowest (A6) in both values. As depicted in Fig. 4, the initial volume was the same in all simulation.

The highest left ventricular pV work was achieved in setting A1 and is $8.6\,\%$ higher than the lowest in setting A6. Work increases with a decreasing α_{endo}, that is the area within pV loops in Fig. 1. The maximal AVPD values spread over a range from $0.54\,$cm for setting A1 to $1.3\,$cm for setting A6 (factor of $241\,\%$). The latter is $21.5\,\%$ higher than in the simulation of [9] and closer to the $1.7\,$cm measured in cine MRI (for details see [9]).

4. Discussion

On the one hand, a significant dependence of SV, EF and AVPD on FO could be observed. Compared to that, the

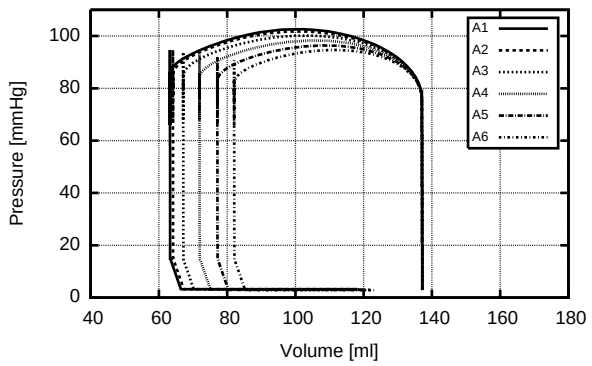

Figure 5. Pressure-volume loop in the left ventricle for the different simulation settings. The area within the curves represents the pressure-volume work.

influence on the pressure difference in the left ventricle is rather small. Results showed that the pressure difference varies by about $8.3\,\%$, whereas ejection fraction shows a larger variation of 34.0%. So, pressure difference is not a reliable sign for the performance of the heart. It could be observed, that the pump function of the heart by means of SV depended significantly (variation of $34\,\%$) on the FO angles. It has to be noted however, that the EFs are significantly lower than values observed in humans (e. g. left ventricle EF $59 \pm 6\,\%$, for 21 untrained male control subjects in [12]). That is the same tendency as found by Carapella et al. [8], they obtained EFs around $45\,\%$.

Apicobasal direction was computed via a potential. It differs from many other methods where the apicobasal direction is computed as the long axis of the left ventricle of the whole heart by a PCA. That is one reason, why the input angles are not directly comparable with experimental data. Thus it is also difficult to compare experimental data of various groups.

The fact that AVPD is a major contributor to the pump function by means of SV could not be observed. In the simulation results, an increasing AVPD goes hand in hand with a decreasing SV, albeit a larger AVPD is generally considered to contribute to SV. Finally, it can be concluded that steeper endocardial fibers contribute more to ventricular pressure, whereas epicardial fibers contribute to AVPD.

References

[1] Streeter DD. Handbook of Physiology: The Cardiovascular System, volume I. American Physiological Society, 1979; 61–112.

[2] Nagler A, Bertoglio C, Gee M, Wall W. Personalization of cardiac fiber orientations from image data using the unscented kalman filter. In Functional Imaging and Modeling of the Heart, volume 7945 of Lecture Notes in Computer Science. Springer Berlin Heidelberg, 2013; 132–140.

[3] Dou J, Reese TG, Tseng WYI, Wedeen VJ. Cardiac diffusion mri without motion effects. Magnetic Resonance in Medicine 2002;48(1):105–114.

[4] Toussaint N. Curvilinear Analysis and Approximation of Cardiac DTI In-Vivo. Phd thesis, King's College London, July 2012.

[5] Krüger MW, Schmidt V, Tobón C, Weber FM, Lorenz C, Keller DUJ, Barschdorf H, Burdumy M, Newher P, Plank G, Rhode K, Seemann G, Sanchez-Quintana D, Saiz J, Razavi R, Dössel O. Modeling atrial fiber orientation in patient-specific geometries: A semi-automatic rule-based approach. In Functional Imaging and Modeling of the Heart, volume 6666 of Lecture Notes in Computer Science. Springer Berlin Heidelberg, 2011; 223–232.

[6] Bayer JD, Blake RC, Plank G, Trayanova NA. A novel rule-based algorithm for assigning myocardial fiber orientation to computational heart models. Annals of Biomedical Engineering 2012;40(10):2243–2254.

[7] Wong J, Kuhl E. Generating fibre orientation maps in human heart models using poisson interpolation. Computer Methods in Biomechanics and Biomedical Engineering 2014;17(11):1217–1226.

[8] Carapella V, Bordas R, Pathmanathan P, Schneider JE, Kohl P, Burrage K, Grau V. Effect of fibre orientation optimisation in an electromechanical model of left ventricular contraction in rat. In Functional Imaging and Modeling of the Heart, volume 7945 of Lecture Notes in Computer Science. Springer Berlin Heidelberg, 2013; 46–53.

[9] Fritz T, Wieners C, Seemann G, Steen H, Dössel O. Simulation of the contraction of the ventricles in a human heart model including atria and pericardium. Biomechanics and Modeling in Mechanobiology 2013;1–15.

[10] Seemann G, Sachse F, Karl M, Weiss D, Heuveline V, Dössel O. Framework for modular, flexible and efficient solving the cardiac bidomain equations using petsc. In Fitt AD, Norbury J, Ockendon H, Wilson E (eds.), Progress in Industrial Mathematics at ECMI 2008, Mathematics in Industry. Springer Berlin Heidelberg, 2010; 363–369.

[11] Guccione JM, Costa KD, McCulloch AD. Finite element stress analysis of left ventricular mechanics in the beating dog heart. Journal of Biomechanics 1995;28(10):1167 – 1177.

[12] Scharhag J, Schneider G, Urhausen A, Rochette V, Kramann B, Kindermann W. Athlete's heart – right and left ventricular mass and function in male endurance athletes and untrained individuals determined by magnetic resonance imaging. Journal of the American College of Cardiology November 2002;40(10):1856–1863.

Address for correspondence:

Lukas Baron
Institute of Biomedical Engineering / Karlsruhe Institute of Technology (KIT)
Fritz-Haber-Weg 1 / D-76131 Karlsruhe / Germany
Lukas.Baron@kit.edu